

ASSESSMENT OF NUMERICAL DIFFUSION EFFECTS IN MAGNETIZED PLASMA PLUME SIMULATIONS

A. Modesti¹, F. Cichocki¹, E. Ahedo¹

¹Equipo de Propulsión Espacial y Plasmas, Universidad Carlos III de Madrid, Leganés, Spain,
Email: alberto.modesti@uc3m.es, filippo.cichocki@uc3m.es, eduardo.ahedo@uc3m.es

KEYWORDS:

EP2PLUS, hybrid PIC-fluid code, magnetized plume, numerical diffusion

ABSTRACT

Magnetized plasma plumes are quite common in electric propulsion applications, both due to internally generated magnetic field for confinement and/or acceleration, and, also in near Earth orbit operations, due to the influence of an arbitrarily inclined geomagnetic field on the plume expansion into vacuum. In order to save computational time, electrons are generally modeled as a fluid, and the corresponding conservation equations are discretized and solved in a given computational mesh. When large anisotropies affect the electron mobility, special care must be taken to reduce or to limit the effect of numerical diffusion. Several codes dedicated to the simulation of magnetized thruster plumes avoid this problem by using a magnetically-aligned mesh, at the cost of more complex algorithms for the mesh generation that may not be worth it. In this work, a method to characterize these numerical diffusion effects in a structured non-magnetically aligned mesh, using the in-house code EP2PLUS, is proposed. It is found that, for angles between the plume axis and the uniform magnetic field between 5 and 30 degrees, the effects of numerical diffusion on the steady state plasma solution are small and do not jeopardize neither the qualitative picture of the self-consistent electron currents and electric fields, nor their quantitative estimation.

1 INTRODUCTION

The present work focuses on the anisotropy existing in conductive fluids, like a plasma, under the effect of a uniform magnetic field, and more specifically, on the numerical analysis of a plasma thruster plume expansion into vacuum. Normally, in such a scenario, only the electrons are “magnetized”, so that the plasma is said to be mesomagnetized. Furthermore, since electrons are generally well confined by electric and magnetic fields, a typical assumption in the modeling of the electron population is to consider electrons as a fluid of a highly anisotropic nature, in which transport in the perpendicular and

parallel directions to the magnetic field is widely different. The classical plasma transport theory states that, for a given plasma density, the perpendicular electron transport coefficient is inversely proportional to the square of the magnetic field strength, B^{-2} and is always smaller, up to various orders of magnitude, than the parallel transport coefficient. These anisotropic transport coefficients may induce a numerical error when numerically solving the flow transport equations, the error becoming more significant if the computational mesh is not aligned with the principal magnetic directions. This numerical error is commonly known as numerical diffusion and its consequences have already been discussed in [1], [2] and [3].

Even in the limit of a perfect confinement, physically possible only in the absence of electron collisions, an undesirable and numerical transfer of particles arises due to the fact that the gradients are computed on mesh nodes that are not aligned with the principal directions of the electron mobility/conductivity tensor. Fig. 1 shows a simplified 2D scenario, in which the electron current is estimated in a non-aligned mesh, from the knowledge of the gradient of a scalar variable Φ , whose iso-lines are parallel to the magnetic field. In the upper red region $\Phi = 1$, and in the lower part $\Phi = 0$ for simplicity, but this can be generalized to any Φ map.

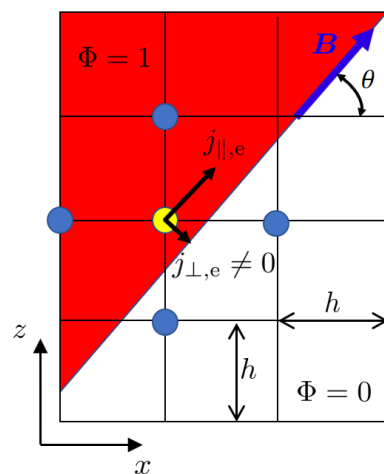


Figure 1: Numerical diffusion effect on a mesh that is not aligned with the magnetic field. A miscalculation of numerical origin in the $j_{\parallel,e}$ leads to a non-zero $j_{\perp,e}$ even in the perfect confinement limit.

The parallel electron current (i.e. along the magnetic field) is then

$$j_{\parallel,e} = \sigma_{\parallel} \partial \Phi / \partial \mathbf{1}_{\parallel}, \quad (\text{Eq. 1})$$

where $\partial \Phi / \partial \mathbf{1}_{\parallel}$ is directional derivative along the magnetic field direction of a scalar variable Φ (which will be later called thermalized potential in Sec. 2.1) and σ_{\parallel} is the high B-parallel conductivity. While the exact value of $\partial \Phi / \partial \mathbf{1}_{\parallel}$ is zero everywhere in this example, the numerical parallel gradient at the yellow point is computed by considering the value of Φ at the 4 blue points shown in the figure. Applying a central difference scheme in a uniform mesh, for the considered Φ map, we have:

$$\frac{\partial \Phi}{\partial \mathbf{1}_{\parallel}} = \cos \theta \frac{\partial \Phi}{\partial x} + \sin \theta \frac{\partial \Phi}{\partial z} \simeq \frac{-\cos(\theta) + \sin(\theta)}{2h}, \quad (\text{Eq. 2})$$

with h representing the uniform mesh spacing along either x or z . Hence, the parallel gradient is generally non-zero (with the isolated exception of $\theta = \pi/4$) and this results in the miscalculation of $j_{\parallel,e}$. Since the electron current density is subject to a continuity equation of the type $\nabla \cdot \mathbf{j}_e = 0$, a spatial variation of the parallel electron current (e.g. between the top blue point where it would be zero, and the yellow point) induces a non-zero perpendicular electron current $j_{\perp,e}$ at the yellow point. Hence, if this were a time marching method, the $\Phi = 1$ side and the $\Phi = 0$ side would slowly merge and the whole domain would finally reach an average value in the steady state.

Apart from increasing the mesh resolution or the discretization order scheme, the only solution to avoid this numerical diffusion is the use of a mesh that is aligned with the preferential directions of the problem; i.e. the principal directions of the conductivity/mobility tensor. Indeed, in the particular case of the electron transport considered here, solving the governing equations in a Magnetic Field Aligned Mesh (MFAM), would avoid a cross-contamination of the transport coefficients and hence numerical diffusion. The assessment of a MFAM and its employment in plasma simulations has been carried out in [4] and [5]. Nonetheless, the numerical diffusion phenomenon has not received much attention in the past, especially in the context of a magnetized plasma plume expanding into vacuum and subject to a uniform geomagnetic field [6]. It is not clear if the added complexity of the magnetically-aligned mesh generation [4] and required algorithms (e.g. for the computation of a scalar gradient in a generally unstructured mesh whose cells can be very irregular [1]) balance or not the use of a non-aligned mesh with a higher resolution. From this point of view, the use of MFAMs has not been properly justified in the literature, and the numerical diffusion effects have rarely been characterized for realistic

simulation scenarios.

In this paper, two simulation scenarios of a magnetized plume expansion will be compared. Simulations with a plasma plume injection along the z axis and a uniform magnetic field at an angle α with it, shall be compared against simulations featuring a magnetic field along z (hence aligned with the mesh) and a plasma plume injection at the same angle α , as shown in Fig. 2. In this figure, $\{X, Y, Z\}$ represents the intrinsic plasma plume reference frame, while $\{x, y, z\}$ is the simulation (fixed structured mesh) reference frame. In order to reproduce the same physical scenario, the angle α between the plume centerline and the magnetic field is the same in both scenarios. While case (b) is unaffected by numerical diffusion effects, case (a) should be affected, so that a direct comparison of the results shown in the intrinsic frame $\{X, Y, Z\}$ should permit to evaluate the numerical diffusion effects, or at least if they are relevant for the considered mesh resolution. The above described simulations will be carried out using our in-house code EP2PLUS [7], which only considers structured meshes. In addition, this work will also aim at validating an oblique field plume expansion case with $\alpha = 30^\circ$, of a previous study on magnetized plasma plumes [6].

The rest of the paper is structured as follows. The magnetized plume model as well as its boundary conditions are described in Sec. 2. Simulation settings and case definitions are illustrated in Sec. 3.1, the main physical aspects of the magnetized plume expansions are presented for different angles in Sec. 3.2, while the numerical diffusion effects are assessed and discussed in Sec. 3.3. Finally, conclusions and future work are summarized in Sec. 4.

2 3D MAGNETIZED PLUME MODEL

As described in [7], hybrid codes represent a very good compromise between accuracy and computational cost, when dealing with the study of plasma plume expansions. The EP2PLUS code (Extensible Parallel Plasma PLUmE Simulator), is a three-dimensional hybrid PIC-fluid code, which was firstly presented at the 2016 Space Propulsion Conference [8]. For this specific study, it is relevant to summarize the magnetized electron fluid model employed in the simulator. Regarding the ions, on the other hand, they are modeled as macro-particles of a particle-in-cell model, and move according to the local electric and magnetic fields. In this work, they are assumed to suffer no collisions with either the fluid electrons or the neutrals (these ones considered as a uniform background).

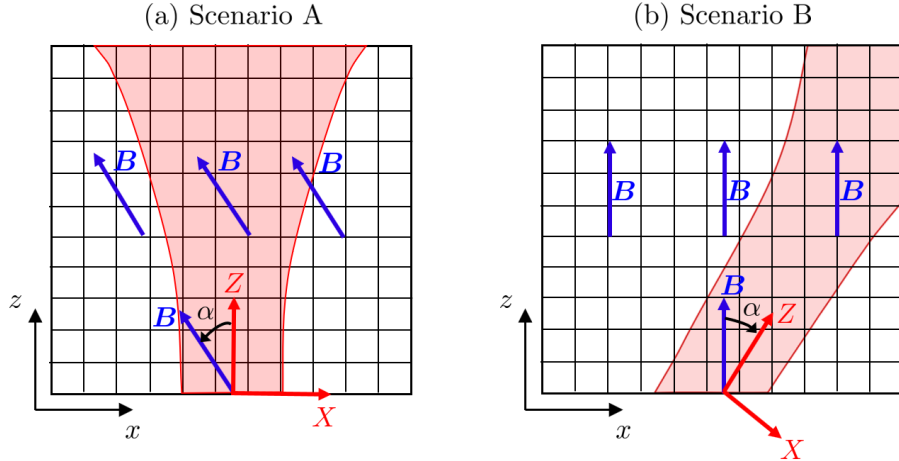


Figure 2: Investigated simulation scenarios for numerical diffusion assessment. Scenario A (a) features a straight plume and an oblique magnetic field, thus not mesh-aligned. Scenario B (b) features an oblique plume injection and a magnetic field aligned with mesh z axis. Thus, in the second scenario, the mesh is magnetically aligned and the simulations should be free of numerical diffusion effects. The red arrows represent the axes of the intrinsic plume reference frame, whose Z -axis always forms the same angle α with the magnetic field direction, so that the depicted scenarios A and B are physically equivalent.

2.1 The magnetized electron model

For a stationary ($\partial/\partial t = 0$) and massless ($m_e \approx 0$) electron fluid, the electron momentum balance equation can be written as:

$$0 = -\nabla \cdot \mathcal{P}_e - e n_e (\mathbf{E} + \mathbf{u}_e \times \mathbf{B}) - \sum_{s=1}^L \nu_{es} m_e n_e (\mathbf{u}_e - \mathbf{u}_s) \quad (\text{Eq. 3})$$

where \mathcal{P}_e is the electron pressure tensor, n_e is the electron number density, m_e is the electron mass, \mathbf{u}_e is the electron fluid velocity, \mathbf{E} is the electric field, \mathbf{B} is an externally applied magnetic induction field, L is the number of heavy particle populations (with which the electrons can collide), and ν_{es} is the momentum transfer collision frequency of the electrons with the generic s^{th} particle population, which features a fluid velocity \mathbf{u}_s .

Let $j_e = -e n_e \mathbf{u}_e$ and $j_i = \sum_{s=1}^L e Z_s n_s \mathbf{u}_s$ be the electron and total ion current density (Z_s and n_s are respectively the charge number and the number density of the generic s^{th} particle population). We define an effective current density grouping collisional effects from heavy species [6] as $j_c = \frac{e n_e}{\nu_e} \sum_{s=1}^L \nu_{es} \mathbf{u}_s$, where $\nu_e = \sum_{s=1}^L \nu_{es}$ is the total electron momentum transfer collision frequency.

Assuming both isotropic and polytropic electrons, $\nabla \cdot \mathcal{P}_e = \nabla p_e$, with $p_e(n_e)$ the scalar electron pressure state law, which allows to introduce a barotropy function h_e , such that $\nabla h_e = \nabla p_e/n_e$. For a given

electron polytropic coefficient γ , we have [7]:

$$h_e(n_e) = -\frac{\gamma T_{e0}}{(\gamma - 1)} \left[1 - \left(\frac{n_e}{n_{e0}} \right)^{\gamma-1} \right], \quad (\text{Eq. 4})$$

where T_{e0}, n_{e0} are the reference electron temperature and density, respectively, at the point where $h_e = 0$.

It is now convenient to define the “residual thermalized potential” Φ , such that $\nabla \Phi = \nabla \phi - \nabla h_e/e$, being ϕ the electric potential. The gradient of the thermalized potential Φ measures the correction to be applied to the Boltzmann relation (generalized to polytropic, non-isothermal electrons), which neglects both magnetic and collisional effects on the electron momentum balance equation. Assuming the same reference zero point for Φ , h_e and ϕ yields:

$$\phi = \Phi + h_e/e. \quad (\text{Eq. 5})$$

So, the electric potential can be retrieved from the knowledge of the barotropic function $h_e(n_e)$ (known from the PIC, in a quasineutral plasma, like the one considered here) and of the thermalized potential Φ , obtained as the solution of a partial differential equation, as detailed below. It is underlined that the near-totality of the existing 3D plume codes neglects the effects of both electron collisions and magnetization, implicitly assuming $\Phi \equiv 0$.

Now, let $\mathbf{1}_b = [b_1, b_2, b_3]$ be the unit vector along the applied magnetic field, so that $\mathbf{B} = B \mathbf{1}_b$, and $\omega_{ce} = eB/(m_e \nu_e)$ the electron gyrofrequency. Then, the Hall parameter is defined as $\chi = \omega_{ce}/\nu_e$. For a finite non-zero total collision frequency, solving Eq. 3 for j_e , substituting all the previous definitions, yields the generalized electron Ohm’s law:

$$\mathbf{j}_e = -\mathcal{K} \cdot (\sigma_e \nabla \Phi + \mathbf{j}_c), \quad (\text{Eq. 6})$$

where the electron scalar conductivity is defined as $\sigma_e = e^2 n_e / (m_e \nu_e)$ and \mathcal{K} is the normalized conductivity tensor, for which $\mathcal{K}^{-1} \mathbf{j} = \mathbf{j} + \chi (\mathbf{j} \times \mathbf{1}_b)$, where

$$\mathcal{K} = \begin{bmatrix} 1 & \chi b_3 & -\chi b_2 \\ -\chi b_3 & 1 & \chi b_1 \\ \chi b_2 & -\chi b_1 & 1 \end{bmatrix}^{-1}. \quad (\text{Eq. 7})$$

In Eq. 6, the thermalized potential gradient is the responsible for numerical diffusion, as it can produce non-physical electron current densities \mathbf{j}_e , when $\nabla \Phi$ is computed in a non-magnetically aligned mesh.

In steady state, the total current density $\mathbf{j} = \mathbf{j}_e + \mathbf{j}_i$ satisfies the continuity equation

$$\nabla \cdot \mathbf{j} = 0, \quad (\text{Eq. 8})$$

which, employing the generalized electron Ohm's law (Eq. 6), becomes an elliptic equation for Φ :

$$\begin{aligned} \mathcal{K} : \nabla \nabla \Phi + \nabla \Phi \cdot (\nabla \cdot \mathcal{K}) \\ + \mathcal{K} \cdot \nabla \Phi \cdot \nabla \ln(\sigma_e) = \frac{\nabla \cdot (\mathbf{j}_i - \mathcal{K} \cdot \mathbf{j}_c)}{\sigma_e} \end{aligned} \quad (\text{Eq. 9})$$

where $\nabla \nabla \Phi$ is the Hessian tensor of the thermalized potential, and $\nabla \cdot \mathcal{K}$ is the divergence of the conductivity tensor.

2.2 Boundary conditions

In order to solve Eq. 9, we set without loss of generality $\Phi = 0$ at one point (e.g. the reference point for the electron properties of the polytropic closure), and prescribe the value of a Φ directional derivative at the boundaries of the simulation domain.

In stationary conditions, the Gauss theorem applied to the simulation volume with $\nabla \cdot \mathbf{j} = 0$, urges that the total net current through the simulation boundary be zero. It is noticed that this condition is valid even during transient conditions, if quasineutrality is assumed ($n_e = \sum_s e Z_s n_s$). A *strong* closure, which satisfies this integral relation, is to impose that the normal electric current density be exactly zero at all boundaries. If $\mathbf{1}_n$ is the normal unit vector at the boundaries, directed towards the plasma domain, from projecting Ohm's law on the normal direction, one obtains:

$$\begin{aligned} \sigma_e (\mathcal{K} \cdot \nabla \Phi) \cdot \mathbf{1}_n &= \sigma_e \nabla \Phi \cdot (\mathcal{K}^T \cdot \mathbf{1}_n) \\ &= (\mathbf{j}_i - \mathcal{K} \cdot \mathbf{j}_c) \cdot \mathbf{1}_n - j_n \end{aligned} \quad (\text{Eq. 10})$$

where $j_n = (\mathbf{j}_e + \mathbf{j}_i) \cdot \mathbf{1}_n$ is the local normal electric current density at the boundary, here set to zero on all boundary surfaces. Eq. 10 imposes the directional derivative of Φ along the direction $\mathcal{K}^T \cdot \mathbf{1}_n$. This

direction is intermediate between the boundary normal ($\mathbf{1}_n$, for $\chi \rightarrow 0$) and the magnetic field direction ($\mathbf{1}_b$, for $\chi \rightarrow \infty$).

3 NUMERICAL SIMULATIONS

3.1 Cases and settings

All relevant physical and computational simulation parameters are summarized in Tab.1. In this study, the plasma is assumed to be quasineutral everywhere ($n_e = \sum_s e Z_s n_s$), so Poisson's equation is not considered.

Two simulations per tilt angle will be carried out, as already commented and shown in Fig.2: one with the magnetic field rotated by an angle α (counter-clockwise) and the plume axis aligned with the z axis (hereafter referred to as scenario A); and a second one with the magnetic field aligned with the z axis and the plume axis rotated by the same angle α (hereafter referred to as scenario B).

Table 1: Simulation parameters.

Simulation parameters	Units	Values
Reference ion density at the origin (n_{e0})	m^{-3}	$1.36 \cdot 10^{16}$
Injected ions profile	n/a	Parks-Katz [9]
Injected Xe ions flow	mg/s	2.38
95% ion current radius	m	0.14
Ions injection axial velocity (u_{inj})	km/s	39.0
Ions initial divergence angle	deg	0.5
Ions injection temperature	eV	0.1
Reference electron temperature (T_{e0})	eV	3.0
Electron polytropic cooling coefficient γ	n/a	1.05
Background neutrals density	m^{-3}	$2.05 \cdot 10^{18}$
Background uniform magnetic induction field magnitude (B)	G	0.5
Upper threshold for the Hall parameter χ	n/a	35
PIC time-step	s	$6.25 \cdot 10^{-8}$
Simulation duration	s	$0.31 \cdot 10^{-3}$
Time-averaging steps for PIC sub-model	n/a	100

Referring to Fig.2, the plume crosses the downstream boundary with different angles in A and B scenarios. Therefore, they are not affected by the same downstream boundary effects and this can make the numerical diffusion assessment harder.

Moreover, the distance traveled by the plume inside the simulation domain would change, for a fixed simulation domain, in scenario B, depending on α . Therefore, in order to obtain a more fair comparison, the magnetized plume solution at a final time instant of 0.31 ms (the same for all angles α) will be considered, at which the plume has not yet reached the lateral or downstream simulation boundary and has covered a fixed distance of slightly more than 12 m along the centerline.

A structured non-uniform rectangular mesh is then adopted, with a uniform spacing along x and y and a linearly increasing one along z . The considered mesh is shown in Fig.3, in the $x - z$ plane ($y = 0$), for both considered scenarios and for $\alpha = 30^\circ$ (the plume centerline is indicated by a red line). The number of nodes along z is always 251, while the z extension depends on the simulation case. As shown in Fig.3, while this is fixed to ~ 20 m in scenario B, in scenario A it depends on α and is chosen so that the plume centerline travels the same distance as in the corresponding oblique plume scenario (B) before reaching the boundary. The mesh extension along y is, on the other hand, always fixed to 2 m with 51 nodes. Regarding the mesh size along x , it is crucial to prevent the plume from reaching the x_{\max} boundary in scenario B, before the final simulation time instant. Therefore, the x extension of the domain is 10 m, with 251 nodes, in scenario B, while it is only 2 m, with 51 nodes, in scenario A. The x and y mesh spacings are thus equal to 4 cm in all simulation scenarios and α cases.

Regarding the plume injection, this follows a Parks-Katz Self-similar profile (SS) [10]. In B scenarios, a rotated profile is employed. This means that the SS solution is first obtained in the *intrinsic plume reference axes* and then interpolated into the employed mesh. The considered tilt angle cases are $\alpha = 5^\circ, 10^\circ, 20^\circ, 30^\circ$ (therefore, 4 α cases, each one subject to 2 simulation scenarios). The last value corresponds to a case that was already investigated in [6]. In simulations with oblique injection and mesh-aligned magnetic field (scenario A), $B_z = B$, and the ion injection fluid velocity features the following components in the simulation reference frame: $u_x = u_{\text{inj}} \sin \alpha$, $u_y = 0$ and $u_z = u_{\text{inj}} \cos \alpha$, where u_x , u_z , are the two relevant components of the ion fluid injection velocity, of magnitude $u_{\text{inj}} = 39$ km/s. The normal injected ion flux, on the other hand is $\Gamma_n = u_z n_{e0}$, with $n_{e0} = 1.36 \cdot 10^{16} \text{ m}^{-3}$ representing the reference plasma density at $x = y = X = Z = 0$. In scenario A, on the other hand, the injection velocity is purely axial, $u_z = u_{\text{inj}}$, while the magnetic field components are: $B_x = -B \sin \alpha$, $B_y = 0$ and $B_z = B \cos \alpha$.

3.2 Reference simulations and general plume characteristics

The plasma plume characteristics can be appreciated, for an unmagnetized case ($B = 0$), in Fig.4 (a),(c),(e) and (g), in terms of the self-consistent electric potential, electron density, ion current and electron current densities, in the meridian plane $y = 0$. The same properties are shown for an oblique injection scenario featuring an injection angle of 5° , in subplots (b), (d), (f) and (h). A classical ambipolar plume expansion with a monotonic potential and density decrease and a globally current-free plasma can be clearly identified. An upstream boundary effect is visible due to the different boundary effects between the straight and oblique injection scenarios, in the electron current density. However, this effect is limited to the lateral regions of the plume, which we are not of interest in this study and do not influence the internal region of the plume.

Results for the magnetized plume with the 4 considered tilt angles can be observed in the $Y - Z$ plane in Fig.5, for scenario A, chosen as a reference for visualization, in terms of the electric current density total magnitude and its component along Z , j_Z .

Considering the typical magnitude of the geomagnetic field (fractions of a Gauss) acting on electron and ions, it can be said that electrons are the only magnetized species, having a Larmor radius smaller than the plume radius by several orders of magnitude. Heavy ions instead can be considered as dimly magnetized, as their gyro-radii are much larger than the plume characteristic size. This difference is relevant when it comes to justify the plume dynamics, and the model adopted for each species, and has, as a direct consequence, the appearance of axial diamagnetic electric current loops, shown in Fig.5. In fact, such loops clearly induce a magnetic field directed out of the page, whereas the applied magnetic field has a component directed into the page. Therefore, the diamagnetic plasma response already detected in [6] is confirmed also at angles between 5° and 30° .

As shown in [6], the axial electric current density has the macroscopic effect of deforming the plasma plume cross section, which, sufficiently downstream, becomes elliptical and more compressed along the direction perpendicular to both the applied magnetic field and the plume centerline. This is induced by a local volumetric force acting on the plume ions given by $j \times B$, and, in this case, by $j_Z B_X$. Therefore, electric currents play a major role in determining the plasma plume response to the applied magnetic field, which has, in turn, a very strong influence on them. For the above reasons, we shall consider the electric current density, and its axial component along the plume centerline as

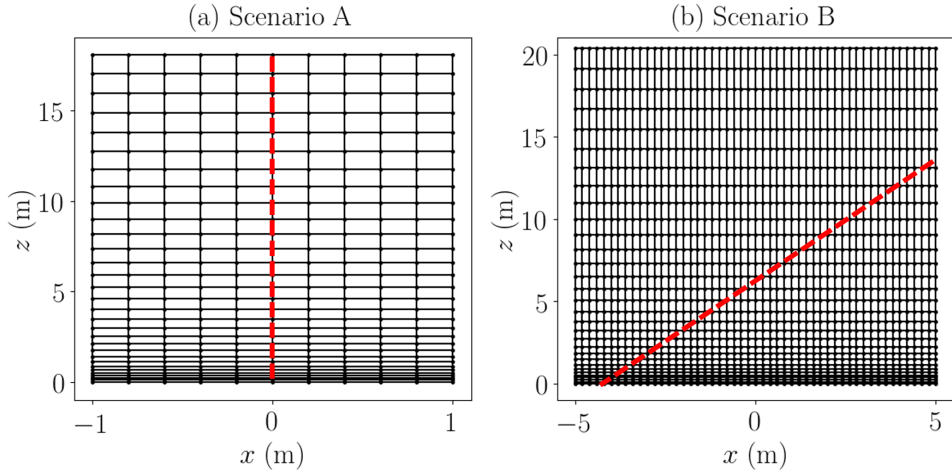


Figure 3: Sketch of the PIC/fluid mesh cross section, at $y = 0$, for the scenarios (a) A and (b) B. The meshes extend for 2 m in the y direction, while the x and z axis scales are not equal. The two meshes are shown for the $\alpha = 30^\circ$ case. The plume centerline in each scenario is indicated by a red line. The black lines represent fixed computational coordinates, and, for the sake of clarity, only one every 5 along x and z are shown (therefore, in reality, more nodes are used).

the most relevant properties to evaluate numerical diffusion effects.

From Fig.5 (b), (d), (f) and (h), it is noticeable that j_Z , and hence the integrated current I_Z flowing in the axial current loops, clearly change with α , as well as the orientation of the separatrix between the two electric current tubes. The latter rotates from an initial direction nearly aligned with the Y axis (at $\alpha = 5^\circ$), to a direction closer to the X axis (at $\alpha = 30^\circ$). This trend would continue until the separatrix becomes parallel to the X direction, for $\alpha = 90^\circ$ (here not considered). Regarding the integrated electric current in the axial current loop, this is provided in Tab.2, and it seems to first decrease with α until 20° , and then increase again, reaching a larger value at $\alpha = 30^\circ$. As shown in [6], the electric current flowing axially should be very small in the aligned plume case ($\alpha = 0^\circ$), so that the trend is non-trivial. An additional simulation for $\alpha = 1^\circ$ case has been carried out, featuring a lower value for I_Z (0.368 vs 0.563 A at 5°). This proves the existence of a complex trend of this axial current versus α .

3.3 Numerical diffusion assessment in the rectangular mesh

In this section, as justified in Sec.3.2, the comparison between scenarios A and B is presented in terms of the electric current density total magnitude in the intrinsic plume plane Y, Z , and its axial component j_Z along the centerline. The latter is compared at $Z = 7$ m.

For these comparisons, the oblique plume injection simulation results have to:

1. be interpolated to the intrinsic plume axes;
2. be rotated in terms of physical vector components to change the coordinate system;

3. and compared with the straight plume one, in terms of contour plots.

Fig.6 shows such a comparison, for the 4 different α values considered here. In this figure, the red lines refer to the solution obtained in scenario B (unaffected by numerical diffusion), while the black lines to the solution obtained for scenario A. The projection of the latter onto the considered plane is shown by a blue arrow in all plots.

Results clearly show that numerical diffusion effects, if present, are quite small, and certainly smaller than boundary effects. In fact, the main differences are observed close to the simulation boundaries, where imposed conditions for the two plume scenarios are physically different. These effects grow with the angle α , and so does the observed differences, which are highest in the highest α case (30°). A grey-shaded region is shown in the j plots to help identify validity regions, sufficiently distant from the boundaries, where the residual differences could be attributed to numerical diffusion. These results also show that, in order to identify more precisely the numerical diffusion effects, a different mesh topology should be considered to have perfectly equivalent boundary conditions, from a physical point of view.

A more quantitative assessment of the numerical diffusion effects or of the observed differences, can be obtained by comparing the axial current flowing in either direction, at $Z = 7$ m (the currents flowing in the positive and negative directions must be equal in magnitude due to current continuity). This axial current is computed by integrating j_Z over the $X - Y$ cross section (see Fig.5, right column) in either the positive or negative regions. As commented before, this variable is associated to the total deformation force acting on the plume ions, and is therefore particularly relevant [6]. The relative difference between these axial currents, in the two simulations scenarios, is reported in Tab.2. This is generally small in

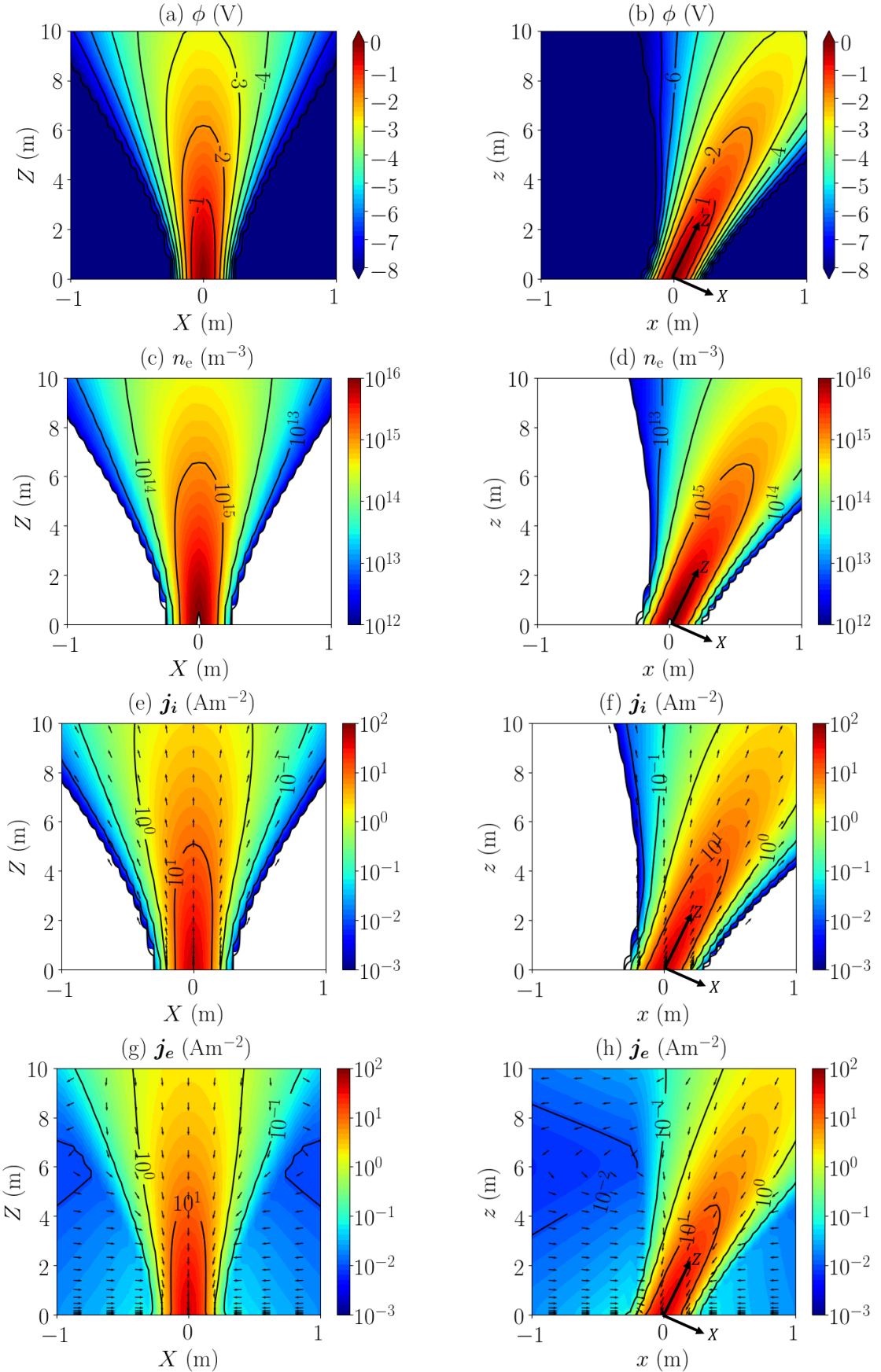


Figure 4: Unmagnetized plasma plume case results at $y = 0$: (a) electric potential, (c) electron density, (e) ion current, and (g) electron current. All properties are symmetric with respect to the plume axis $X = Y = 0$, so the $X = 0$ cross sections have been omitted. (b), (d), (f) and (h) refer to an inclined plume of 5° and are shown in the $x - z$ plane. The x and z axis scales in the figure are not equal, thus the oblique plume appears slightly asymmetrical.

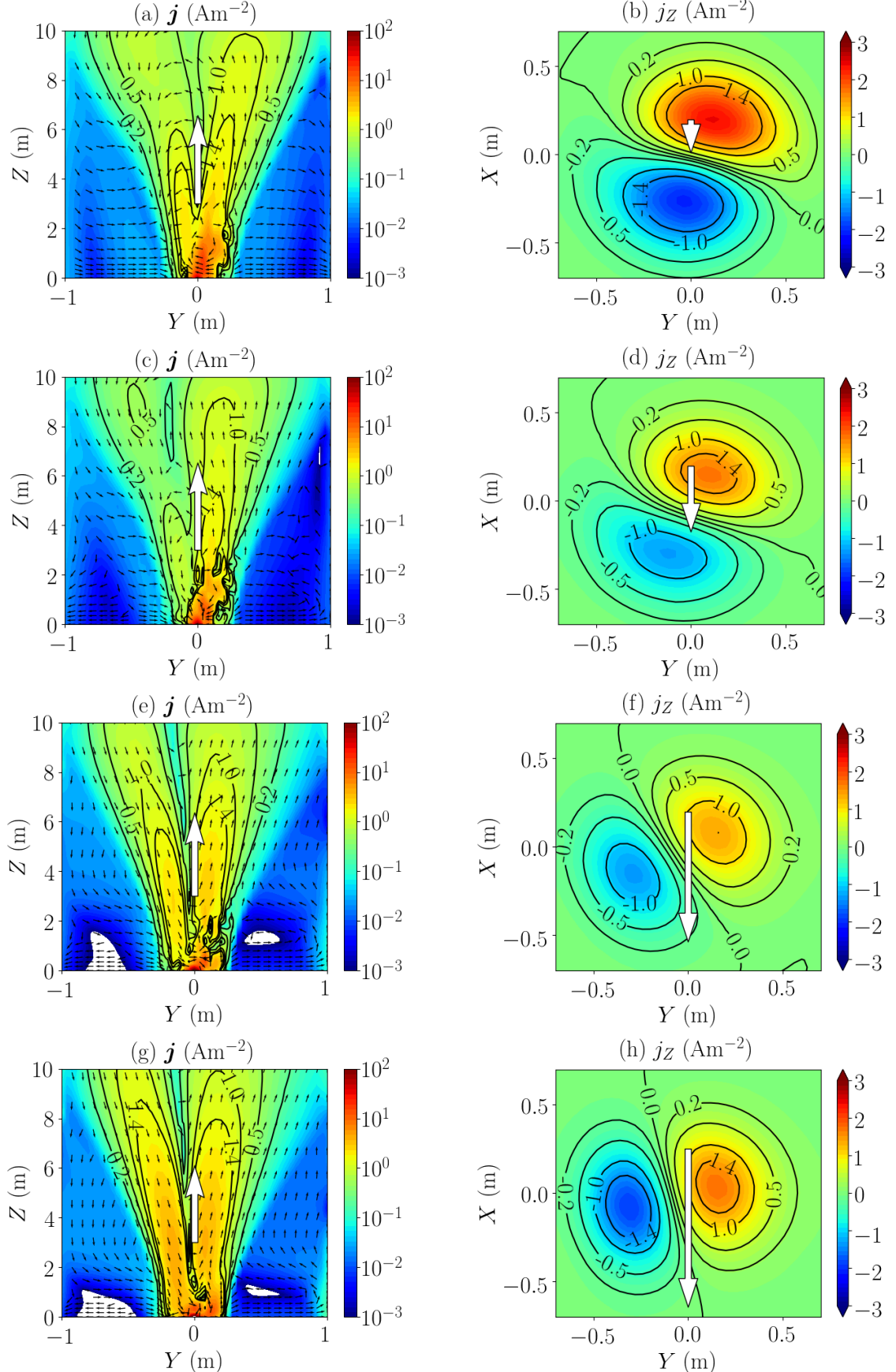


Figure 5: Results for the electric current density \mathbf{j} (left column) in the $Y - Z$ plane, and its axial component j_z at $Z = 7 \text{ m}$ (right column) for different tilt angles α : (a) and (b) 5° , (c) and (d) 10° , (e) and (f) 20° , (g) and (h) 30° . Only results for scenario A are shown, as scenario B results are nearly the same in the considered intrinsic reference frame $\{X, Y, Z\}$. A white arrow indicates the projection of the magnetic field direction onto the considered plane. This field always belongs to the $X - Z$ plane. In the j_z subplots, a positive value of the current density means that it enters the page (just like the magnetic field, which has a positive Z component). In \mathbf{j} subplots, the magnetic field component along X is negative and hence directed into the page.

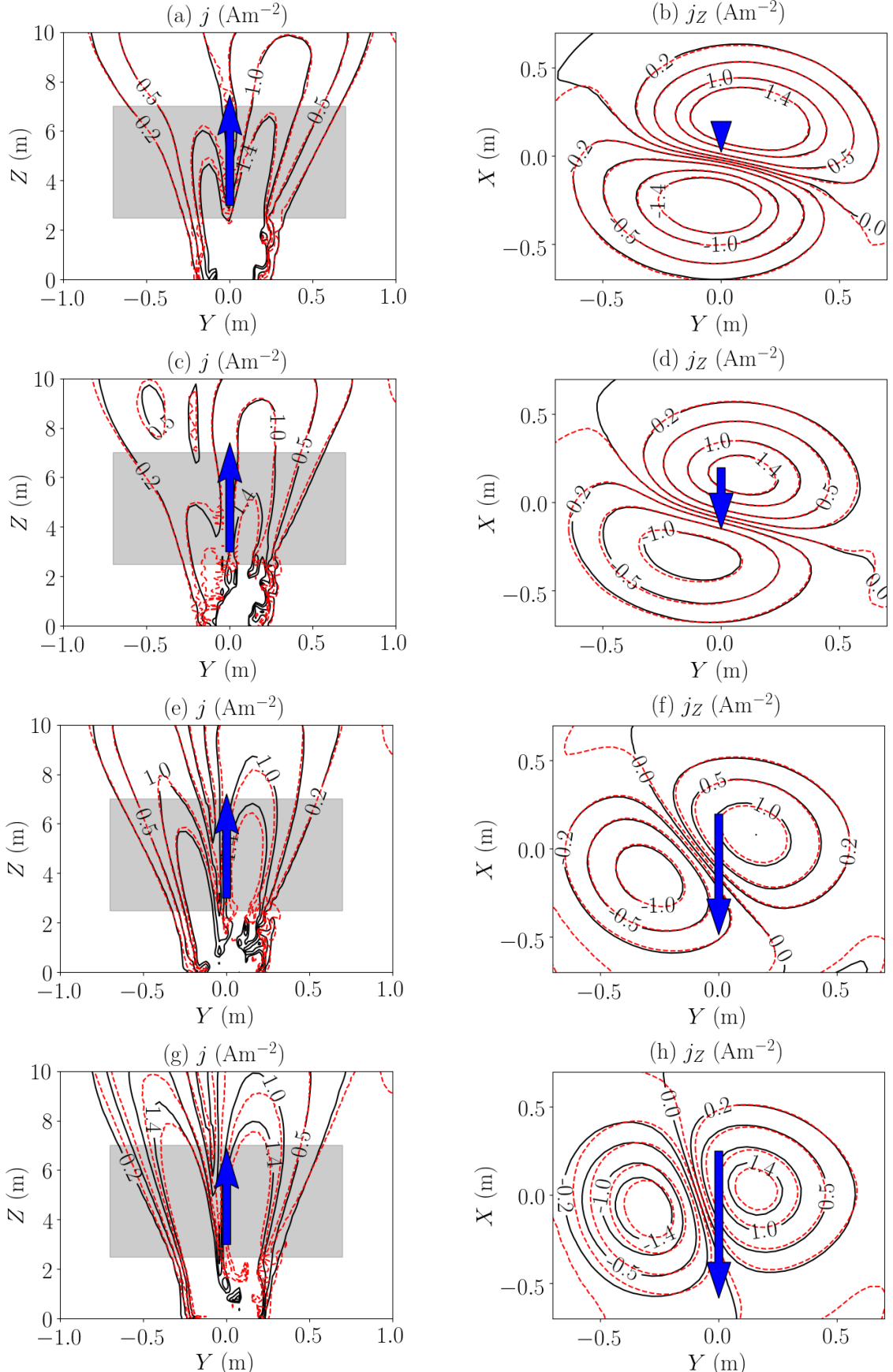


Figure 6: Comparison plots for the electron current density magnitude j (subplots (a), (c), (e) and (g)) and for its Z -component j_Z , at $Z = 7 \text{ m}$ (subplots (b), (d), (f) and (h)), for the 4 different magnetic field tilt angles α : (a)-(b) 5° , (c)-(d) 10° , (e)-(f) 20° , (g)-(h) 30° . Red dashed lines represent the scenario B solution, while black solid lines represent the solution in scenario A, theoretically affected by numerical diffusion. The magnetic field projection onto the considered plane is shown by a blue arrow. A grey-shaded region is shown in the j plots to help identify validity regions.

all tilt angle cases and may not be attributed entirely to numerical diffusion effects, as the difference between boundary effects might still be playing a role at the considered cross section. In any case, the reported differences can be considered as an upper threshold for assessing the numerical diffusion effects, which, for a maximum Hall parameter of 35, do not produce a difference of more than a few percent points in the axial current.

Table 2: Relative (percentage) error between the current flowing in the axial current tubes at $Z = 7$ m, in scenarios A and B. Reported values refer to the final simulation time, $t = 0.31$ ms, (or timestep 5000), at which the plume has covered a distance of ~ 12.5 m.

Case	I_Z [A] (scenario A)	I_Z [A] (scenario B)	ΔI_Z (%)
5°	0.567	0.559	1.4%
10°	0.393	0.398	1.3%
20°	0.329	0.340	3.3%
30°	0.411	0.417	1.4%

The above described analysis, nevertheless, has its own limitations. First of all, it refers to a steady state scenario, with no temporal terms. Therefore numerical diffusion effects on j_e , if present, cannot propagate in time. In addition, simulations have been carried out for a maximum Hall parameter equal to 35 (obtained by setting a minimum uniform neutral background density), for numerical convergence reasons, i.e. in order to reduce the numerical truncation error of the finite differences scheme, while maintaining a reasonable mesh resolution. A higher value for the limiting value of χ yields to higher magnetized electron effects and hence a larger numerical diffusion. However, it was shown in [6] that, as the maximum Hall parameter is increased, the solution quickly reaches an asymptotical trend and saturates at values not much larger than 100. Therefore, the solution for a non-limited χ parameter would not diverge from the one shown here.

This work, albeit limited in its application and generality, has however permitted to advance in developing appropriate techniques for evaluating numerical diffusion effects in realistic magnetized plasma plume simulations on structured meshes, and to evaluate as negligible, both qualitatively and numerically, the numerical diffusion effects in a case of interest ($\alpha = 30^\circ$), which was analyzed in a previous study [6].

4 CONCLUSIONS AND FUTURE WORK

This paper has presented a numerical diffusion analysis in the context of a magnetized plasma

plume expansion. Appropriate structured and non-uniform rectangular meshes have been adopted in order to guarantee a mesh-aligned and non-aligned magnetic field, as well as a partial mitigation of boundary effects in the bulk region of the plasma plume. An oblique injection algorithm for a self-similar plume profile was implemented in order to obtain a tilted plume injection with respect to the considered structured mesh directions. This allowed to obtain two physically quasi-equivalent scenarios presenting the same angle between the plume centerline and the magnetic field: one theoretically affected by numerical diffusion (non-aligned field case, straight plume injection) and another one with no such effect (aligned field, oblique plume injection).

In order to evaluate the numerical diffusion effects, four tilt angles α between the plume centerline and the magnetic field have been considered, ranging from 5° to 30° . The effects of the external magnetic field have been identified mainly in terms of the electric current density and its component along the plume centerline, for both a qualitative and quantitative comparison. It has been found that the mesh-field misalignment does not generate a relevant numerical diffusion and the solution is not corrupted significantly by it. In fact, the main differences are found in regions close to the simulation boundaries, which can introduce relevant differential effects between the two considered scenarios and grow with the tilt angle.

The EP2PLUS simulator is therefore capable of reproducing a magnetized plume expansion on a non-aligned structured mesh, with a sufficiently small numerical diffusion. Nevertheless, this has been verified only for a steady-state plasma plume scenario, with an upper-limited Hall parameter, and hence a limited magnetization ($\chi \sim 35$). Without this artificial upper limit, the numerical diffusion effects might be larger than those observed here, although a previous study suggests that they saturate quickly with χ , so that they are not expected to alter drastically the conclusions reached here.

Future work will focus on the following topics: (i) the assumption of a lower neutral background density to have greater electron magnetization effects, (ii) the consideration of additional tilt angles between the magnetic field and the plume axis, going from a nearly parallel to a nearly perpendicular scenario, and (iii) the adoption of a more extended mesh, with a different geometry to further reduce the effects of the simulation boundaries. Regarding the last mentioned topic, in order to limit the different boundary effects at higher α values, an oblique plume injection in both simulation scenarios can be considered, but with a mesh tilted by the same angle as the plume

in the non-aligned field simulation case. Thus, the plume will cross both the upstream and downstream boundaries with the same angle, and will be subject to the same boundary effects. This would be extremely important when the latter are not negligible (i.e. for $\alpha \geq 30^\circ$) and cannot be easily distinguished from numerical diffusion errors.

ACKNOWLEDGMENTS

The research has been funded by the Comunidad de Madrid, grant agreement Y2018/NMT-4750 (PROMETEO-CM).

REFERENCES

- [1] Pérez-Grande, D., González-Martínez, O., Fajardo, P., and Ahedo, E., “Analysis of the numerical diffusion in anisotropic mediums: benchmarks for magnetic field aligned meshes in space propulsion simulations,” *Applied Sciences*, Vol. 6, No. 11, 2016, pp. 354.
- [2] Meier, E., Lukin, V., and Shumlak, U., “Spectral element spatial discretization error in solving highly anisotropic heat conduction equation,” *Computer Physics Communications*, Vol. 181, No. 5, 2010, pp. 837–841.
- [3] Anderson, D. V., “Axisymmetric multifluid simulation of high beta plasmas with anisotropic transport using a moving flux coordinate grid,” *Journal of Computational Physics*, Vol. 17, No. 3, 1975, pp. 246–275.
- [4] Zhou, J., Pérez-Grande, D., Fajardo, P., and Ahedo, E., “Numerical treatment of a magnetized electron fluid within an electromagnetic plasma thruster code,” *Plasma Sources Science and Technology*, Vol. 28, No. 11, 2019, pp. 115004.
- [5] Araki, S. and Wirz, R., “Magnetic Field Aligned Mesh for Ring-Cusp Discharge Chambers,” *50th AIAA/ASME/SAE/ASEE Joint Propulsion Conference & Exhibit*, No. AIAA 2014-3830, Cleveland, Ohio, US, 2014.
- [6] Cichocki, F., Merino, M., and Ahedo, E., “Three-dimensional geomagnetic field effects on a plasma thruster plume expansion,” *Acta Astronautica*, Vol. 175, 2020, pp. 190 – 203.
- [7] Cichocki, F., Domínguez-Vázquez, A., Merino, M., and Ahedo, E., “Hybrid 3D model for the interaction of plasma thruster plumes with nearby objects,” *Plasma Sources Science and Technology*, Vol. 26, No. 12, 2017, pp. 125008.
- [8] Cichocki, F., Domínguez, A., Merino, M., and Ahedo, E., “A 3D hybrid code to study electric thruster plumes,” *Space Propulsion Conference 2016*, No. paper 2016-3124968, Association Aéronautique et Astronautique de France, Rome, Italy, May 2-6, 2016.
- [9] Parks, D. and Katz, I., “A preliminary model of ion beam neutralization,” *14th International Electric Propulsion Conference*, paper 1979-2049, Electric Rocket Propulsion Society, Fairview Park, OH, Princeton, New Jersey, October 30 - November 1, 1979.
- [10] Merino, M., Cichocki, F., and Ahedo, E., “Collisionless Plasma thruster plume expansion model,” *Plasma Sources Science and Technology*, Vol. 24, No. 3, 2015, pp. 035006.